ARTICLE IN PRESS

High Energy Density Physics xxx (2010) 1–11

Contents lists available at ScienceDirect

High Energy Density Physics

journal homepage: www.elsevier.com/locate/hedp

Superconfiguration widths and their effects on atomic models

Stephanie B. Hansen [a,*], Jacques Bauche [b], Claire Bauche-Arnoult [b]

[a] Sandia National Laboratories,Albuquerque, NM 87185, USA
[b] Laboratoire Aimé Cotton, Campus d'Orsay, Bâtiment 505, 91405 Orsay, France

ARTICLE INFO

Article history:
Received 13 May 2010
Received in revised form
20 July 2010
Accepted 22 July 2010
Available online xxx

Keywords:
Collisional-radiative
Non-LTE
Spectroscopic

ABSTRACT

Superconfigurations are an important component of many of the collisional-radiative atomic models that are used to predict the properties of atoms and ions in non-local thermodynamic equilibrium (non-LTE) plasmas. In this paper, we investigate the statistical properties of superconfigurations and derive expressions for their approximate average energies and energy variances based on one-electron orbital energies. We also explore the effects of using finite-width superconfigurations in screened hydrogenic and hybrid-structure atomic kinetics models.

© 2010 Published by Elsevier B.V.

1. Introduction

Collisional-radiative atomic models are widely used in high-energy-density plasma science, from the compact inline atomic models used in hydrodynamics codes [1–3] to the detailed fine-structure models used for spectroscopic plasma diagnostics [4–7]. Code comparisons performed at a series of non-LTE workshops [8–12] have established the importance of statistical completeness for model accuracy and reliability, particularly completeness in the dielectronic recombination channels that control the ionization balance of multi-electron ions in non-LTE plasmas. (For our purposes, a statistically complete model is one whose predictions do not change upon addition of energy levels.) Since the statistical weight required to model a "complete" ion grows exponentially with the number of electrons, reliable non-LTE calculations of complex ions pose a significant computational challenge.

One highly successful class of statistically complete atomic kinetic models uses screened hydrogenic superconfigurations whose states $(n_1)^{N_1}(n_2)^{N_2}\ldots(n_k)^{N_k}$ are described by their principal quantum numbers n and their integer occupation numbers N [2,3,13]. Each such superconfiguration (SC) can carry enormous statistical weight, thus enabling statistical completeness for arbitrarily complex ions at a modest computational cost. The screened hydrogenic approach has proven to be quite general and powerful for reasonably accurate calculations of charge state distributions. Coupled with tabular data for line transitions from more detailed codes [14,15], screened hydrogenic models can even generate reasonable emission and absorption spectra.

An alternative approach to non-LTE calculations involves the generation of an extensive set of detailed atomic data based on *nl*, *nlj* or even fine structure energy levels. These data are more accurate than screened-hydrogenic SCs and can be ensemble-averaged into a more tractable data set before solving the collisional-radiative rate matrix. Researchers have explored various paths to optimizing approaches like this for accuracy and efficiency, including dynamically varying the ensembles according to plasma conditions [16–19], expanding ensembles after the matrix solution to determine more detailed state populations [20–22], determining plasma-dependent effective temperatures within ensembles [23–25], averaging only high-*n* SCs [26,27], or using hybrid atomic structure designed for fidelity in both the high- and low- density plasma regimes [28,29]. Although these approaches can yield reliable charge state distributions and even generate highly accurate synthetic spectra, only highly averaged and hybrid-structure kinetic models can be extended to ions of arbitrary complexity without sacrificing completeness or becoming computationally intractable (*c.f.* Ref. [30]).

Energy levels are the fundamental components of all these atomic models. But only fine-structure energy levels are "simple," completely defined by their binding energy and their degeneracy (and even fine structure states are simple only in the absence of

* Corresponding author. Tel.: +1 505 844 1298.
E-mail address: sbhanse@sandia.gov (S.B. Hansen).

1574-1818/$ – see front matter © 2010 Published by Elsevier B.V.
doi:10.1016/j.hedp.2010.07.002

Please cite this article in press as: S.B. Hansen, et al., Superconfiguration widths and their effects on atomic models, High Energy Density Physics (2010), doi:10.1016/j.hedp.2010.07.002

external electric and magnetic fields). All other representations of energy levels (*nl*, *nlj*, or SC) are ensembles that generally contain, either implicitly or explicitly, additional structure due to the fine-structure states they comprise. This internal complexity is most obviously manifested in the poor-quality spectra of highly averaged models, and much effort has been devoted to understanding the statistical properties of transition arrays so that reasonable spectra can be generated with tractable models [21,31–33]. However, a majority of that effort has focused on LTE and near-LTE plasmas whose internal populations follow Boltzmann statistics and on non-LTE models whose energy levels are already moderately detailed (*e.g. nl* configurations in Ref. [34]) or whose internal structure is explicitly acknowledged [23–25]. Less attention has been paid to the consequences of treating large ensembles of energy levels as simple states void of internal structure in plasmas far from equilibrium. We might expect these consequences to be most obvious in the screened hydrogenic models whose superconfigurations can represent tens of thousands of fine structure levels [35]; this will be the focus of the present paper.

We begin in Section 2 by investigating the average energies and energy variances of superconfigurations, proposing simple formulas for these quantities based on one-electron orbitals and comparing these estimates to the results of more detailed calculations. In Section 3, we investigate the consequences of non-zero SC widths on continuum lowering in dense plasmas, dielectronic recombination in complex ions and beam plasmas, and hybrid-structure models that couple screened hydrogenic SCs to detailed levels. Finally, we illustrate the effects of finite-width SCs on bound-free absorption edges in Section 4.

2. Statistical properties of superconfigurations

In this section, we investigate the average energies and energy variances of superconfigurations. For any case where a complete set of detailed level data for a superconfiguration is known, the average energy $\langle E\rangle_{\mathrm{SC}}$ of that SC is:

$$\langle E\rangle_{\mathrm{SC}} = \frac{\sum_i g_i E_i}{\sum_i g_i} \tag{1}$$

and the energy variance is given by:

$$\sigma^2_{\mathrm{SC}} = \frac{\sum_i g_i [E_i - \langle E\rangle_{\mathrm{SC}}]^2}{\sum_i g_i} \tag{2}$$

with σ_{SC} the standard deviation, E_i the energy of a detailed level, and g_i its statistical weight. Here, the detailed levels can be fine structure states, relativistic configurations, non-relativistic configurations, or any mixture of such states, as long as the states are completely enumerated for the SC ensemble.

Alternatively, one can define approximate orbital-based expressions for the average energy and energy variance of a superconfiguration that do not require a complete enumeration of the sub-states within a given SC. Instead, the orbital approximation requires only the one-electron binding energies E_{nl} [36] of the non-relativistic orbitals that contribute to the SC. These can be calculated by finding the solutions of the Schrödinger equation in a Hartree-type approach or approximated by the single-electron energies $E_{nl} \approx \partial E^{\mathrm{tot}}_{\mathrm{SHM}}/\partial P_{nl}$ of an *nl*-dependent screened hydrogenic model such as the one described in [37,38] With statistical weights $g_{nl} = 2(2l+1)$, the average energy and energy variance of the one-electron orbitals of an *n* shell are:

$$\langle E\rangle_n = \frac{1}{2n^2}\sum_l g_{nl} E_{nl} \tag{3}$$

and

$$\begin{aligned}\sigma_n^2 &= \frac{\sum_l g_{nl}[E_{nl} - \langle E\rangle_n]^2}{\sum_l g_{nl}} \\ &= \left(\frac{\sum_l g_{nl}E_{nl}^2}{\sum_l g_{nl}}\right) - \left(\frac{\sum_l g_{nl}E_{nl}}{\sum_l g_{nl}}\right)^2 \\ &= \left\langle E^2\right\rangle_n - \langle E\rangle_n^2\end{aligned} \tag{4}$$

Similar formulas can be defined for relativistic one-electron orbital energies E_{nlj} with $g_{nlj} = 2j+1$ by changing the sum over *l* to a sum over relativistic orbitals κ. Either approach will yield a set of $\langle E\rangle_n$ and σ_n^2 that vary by ion. The energy of a single-shell superconfiguration $(n)^N$ is given by the sum

$$\langle E\rangle_{(n)^N} = N\langle E\rangle_n \tag{5}$$

The energy variance of the SC $(n)^N$ can be approximated by constructing configuration energies based on one-electron orbital energies E_{nl}, followed by application of the straightforward formulas given above in Eqs. (1) and (2). Consider the superconfiguration $(2)^3$. This SC contains the configurations $2s^22p$, $2s2p^2$, and $2p^3$, with respective energies of $(2E_{2s} + E_{2p})$, $(E_{2s} + 2E_{2p})$, and $(3E_{2p})$ and statistical weights of 6, 30, and 20. The energy variance of these configurations calculated by Eq. (2) yields the polynomial $\sigma^2 = (15/112)\,(3E_{2s}^2 + 3E_{2p}^2 - 6E_{2s}E_{2p})$. A general and compact form of this expression for the variances is:

$$\sigma^2_{(n)^N} = \frac{N(2n^2 - N)}{n^4(2n^2-1)}x(n) \tag{6}$$

$$\begin{aligned}x(n) &= \sum_{l=0}^{n-1}\left[\left(2l+1\right)n^2 - (2l+1)^2\right]E_{nl}^2 \\ &\quad - \sum_{l=0}^{n-1}\sum_{l'=0}^{n-1}(2l+1)(2l'+1)E_{nl}E_{nl'} \quad \text{with } l \neq l'\end{aligned} \tag{7}$$

The non-relativistic polynomials for $n = 2$–4 are:

$$x(2) = 3E_{2s}^2 + 3E_{2p}^2 - 6E_{2s}E_{2p}$$

$$x(3) = 8E_{3s}^2 + 18E_{3p}^2 + 20E_{3d}^2 - 6E_{3s}E_{3p} - 10E_{3s}E_{3d} - 30E_{3p}E_{3d}$$

$$\begin{aligned}x(4) &= 15E_{4s}^2 + 39E_{4p}^2 + 55E_{4d}^2 + 63E_{4f}^2 - 6E_{4s}E_{4p} - 10E_{4s}E_{4d} \\ &\quad - 14E_{4s}E_{4f} - 30E_{4p}E_{4d} - 42E_{4p}E_{4f} - 70E_{4d}E_{4f}\end{aligned}$$

For relativistic orbitals, the coefficient remains the same but the polynomial $x(n)$ changes to a relativistic version $x^{\mathrm{rel}}(n)$, with the sum over *l* changing to a sum over relativistic orbitals *lj*, here indexed by κ:

$$\begin{aligned}x^{\mathrm{rel}}(n) &= \sum_{\kappa}\left[(j+1/2)n^2 - (j+1/2)^2\right]E_\kappa^2 \\ &\quad - \sum_{\kappa}\sum_{\kappa'}(j+1/2)(j'+1/2)E_\kappa E_{\kappa'} \quad \text{with } \kappa \neq \kappa'\end{aligned} \tag{8}$$

The relativistic polynomial for $n = 2$ is:

$$\begin{aligned}x^{\mathrm{rel}}(2) &= 3E_{2s_{\frac{1}{2}}}^2 + 3E_{2p_{\frac{1}{2}}}^2 + 4E_{2p_{\frac{3}{2}}}^2 - 2E_{2s_{\frac{1}{2}}}E_{2p_{\frac{1}{2}}} - 4E_{2s_{\frac{1}{2}}}E_{2p_{\frac{3}{2}}} \\ &\quad - 4E_{2p_{\frac{1}{2}}}E_{2p_{\frac{3}{2}}}\end{aligned}$$

Please cite this article in press as: S.B. Hansen, et al., Superconfiguration widths and their effects on atomic models, High Energy Density Physics (2010), doi:10.1016/j.hedp.2010.07.002

This reduces to the non-relativistic $x(2)$ when $E_{2p1/2} = E_{2p3/2} = E_{2p}$. We note that one cannot obtain relativistic variances by performing a statistically weighted average of E_{nlj} to obtain E_{nl} and then using the non-relativistic $x(n)$; this leads to an incorrect weighting of the E_{nlj} that gives a smaller variance than E_{nlj} and $x^{rel}(n)$.

In the orbital approximation, the energy variance of a superconfiguration with multiple open shells $(n_1)^{N_1}(n_2)^{N_2}\ldots(n_k)^{N_k}$ is given by the sum of the variances for each shell (*c.f.* [39]):

$$\sigma_{SC}^2 = \sum_k \sigma^2(n_k)^{N_k} \tag{9}$$

The average energies of composite SCs are simply

$$\langle E\rangle_{SC} = \sum_k \langle E\rangle_{(n_k)^{N_k}} \tag{10}$$

Fig. 1 shows the structure of selected SCs in Ge^{16+} (ground SC $(3)^6$) and Ge^{17+} (ground SC $(3)^5$) as calculated by AVERROES [34] to illustrate the behavior of composite SC energies and widths within and between ions. The minimum, average, and maximum energies of configurations within the listed SCs are indicated, measured with respect to the lowest-energy configuration in Ge^{16+}. The energy difference between the lowest- and highest-energy configurations within each SC is generally about 6σ. The widths do not vary much between adjacent ions, nor is there large variation in the widths of composite SCs formed by single and even double excitations from the M-shell. In contrast, inner-shell holes from $n = 2$ increase the widths significantly. The absolute widths of these SCs are of the same order as or much larger than their energy differences, illustrating the underlying structure that is absent in zero-width SC representations of complex ions.

2.1. Numerical comparisons of the SC average energies and variances

Fig. 2 shows the average energies $\langle E\rangle_{SC}$ and standard deviations σ_{SC} for the ground SCs of L-shell aluminum ($Z = 13$), germanium ($Z = 32$), and xenon ($Z = 54$), as computed using one-electron orbital energies. Here, the non-relativistic one-electron orbital energies were computed by the MUZE code [40] and the relativistic orbital energies were computed by LIMBO [15]. Also given are σ_{SC} obtained by the straightforward application of Eq. (2) to the ensembles of energy levels within those SCs as computed by the relativistic atomic structure code FAC [5]. Computations using relativistic configurations (designated "UTA" for Unresolved Transition Array mode) and fine structure ("FS") levels with and without full configuration interaction (CI) are shown. The plots of $\langle E\rangle_{SC}$

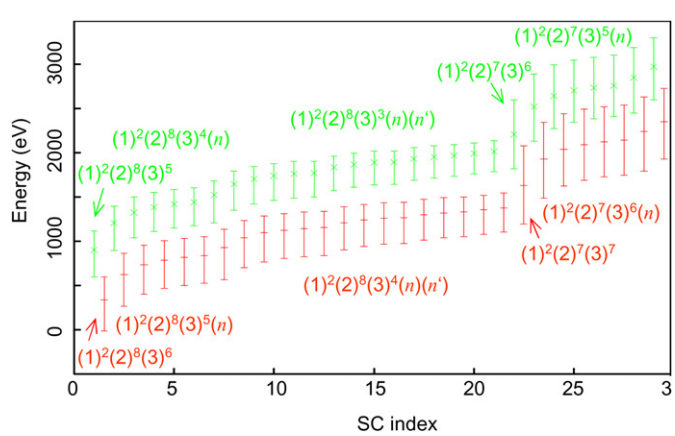

Fig. 1. Minimum, maximum, and average configuration energies in selected SCs of Ge^{16+} and Ge^{17+} ions [34].

illustrate that relativistic effects are significant for Ge and Xe and that fine structure and configuration interaction effects are most pronounced for Al. Generally, the UTA σ_{SC} are the smallest of the FAC calculations, with increasing energy widths obtained as fine structure and configuration interaction effects are included. For the highly charged xenon ions, the relativistic orbital-based expression gives excellent agreement with FAC. The agreement is reasonable for the lower-charged ions. Also shown for the Ge case are data from the atomic structure code AVERROES [34], which uses non-relativistic orbitals with relativistic corrections and determines σ_{SC} directly from Eq. (2).

Fig. 3 gives $\langle E\rangle_{SC}$ and σ_{SC} for the M-shell ions of copper and tungsten. As with the L-shell case, relativistic effects are important for the higher-Z element, but in this case we find that FS and CI effects on the statistical properties of the SCs are small, even for the lower Z. The orbital-based expression for σ_{SC} agrees very well with both FAC and AVERROES data. For both the L- amd M-shell cases, the typical energy widths of the open-shell ground superconfigurations can approach or even exceed energy differences between ions, as was shown in Fig. 1.

The one-electron orbital approximations for $\langle E\rangle_{SC}$ and σ_i given in Eqs. (9) and (10) can be used to construct Gaussian distributions of statistical weight with energy:

$$g(E) = \frac{g_{SC}}{\sigma\sqrt{2\pi}} e^{\frac{-(E-\langle E\rangle_{SC})^2}{2\sigma^2}} \tag{11}$$

Fig. 4 illustrates how the approximate $g(E)$ correspond to those of detailed calculations from FAC. We caution that the exact form of the FAC distributions is sensitive to the selection of the energy bins, especially for the ions with smaller total statistical weights g_{SC} (as listed on the figure). The orbital-based statistical representations are most accurate for complex ions with large statistical weights, but give a reasonable representation for $g(E)$ overall.

3. Effects of SC widths on non-LTE atomic kinetics

In this section, we explore the consequences of applying the estimates given above for the average energies and energy variances of superconfigurations to the non-LTE kinetics of SC-based screened hydrogenic models. While such models can never attain the fidelity of models with more detailed representations of the atomic structure, their huge advantages in tractability, generality, and completeness make them attractive and we are interested in optimizing them as far as possible. Because we wish to apply our arguments to screened hydrogenic SCs of arbitrary complexity (or simplicity), much of the discussion below will be qualitative, glossing over the particularities of specific transition arrays and in general assuming that SCs with similar $\langle E\rangle$ have similar σ.

Previous studies of rates between ensembles of detailed levels [41] have established two general correlation laws that describe the behavior of transitions between the elements of coupled ensembles.

(1) Propensity: if some process links the elements (levels or configurations) of superconfigurations SC and SC′, the higher (lower) levels of SC are linked by larger rates to the higher (lower) levels of SC′, than to its lower (higher) levels.
(2) Strengths: the total rate of atomic transfer from an element i of the initial SC to the whole of SC′ is an increasing-linear function of E_i(SC).

These correlations hold for radiative, collisional, and even two-electron transitions. And they provide some justification

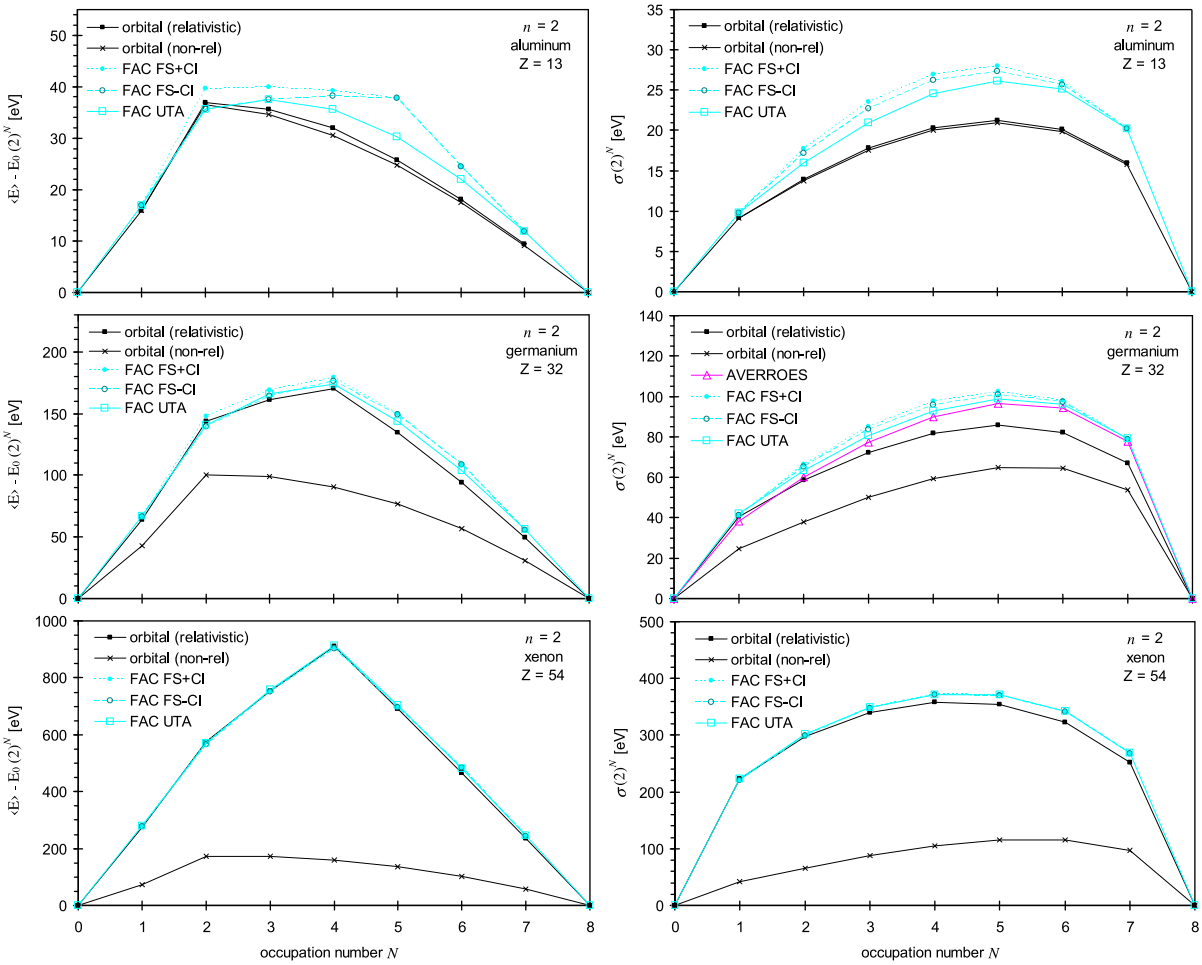

Fig. 2. Average energies (left) and standard deviations (right) in eV of various superconfigurations in the L-shells of aluminum, germanium, and xenon. Values computed from the detailed FAC [5] and AVERROES [34] atomic structure codes are given in cyan and magenta, respectively. The average energies are given relative to the lowest-energy state within the SC.

for the general success of zero-width SC models: consider the case of two coupled superconfigurations SC and SC′, each composed of k configurations c_i and c'_i. If the first correlation law (based on the fact that the spectator nl subshells must be the same in both SCs [23,24]) holds strictly, then exactly k rates couple SC and SC′.

By the second correlation law, the rates R_i scale linearly with the energies of the initial configurations, so that if $\langle E\rangle R$ is proportional to some typical rate at the average energy $\langle E\rangle$ of the initial SC, then the global rate between SC and SC′ obtained by taking a statistically-weighted average of E_iR over c_i and a sum over $c'_{i'}$ is identically $\langle E\rangle R$. Thus, rates between SCs are well represented by the screened hydrogenic rates calculated using the difference in their average energies $\Delta\langle E\rangle R$.

A similar argument holds even for SC pairs that have significant energy overlap, as illustrated in Fig. 5 for the first two excited SCs of neutral Al. The global rates between such SCs should be reasonably close to the screened hydrogenic rates calculated using $\Delta\langle E\rangle R$ (illustrated by the dashed line). However, strongly overlapping SCs open up the possibility of decay rates from SCs with lower average energies to SCs with higher average energies (illustrated by the two dotted lines). For example, in neutral aluminum, the 5s orbital is more tightly bound than 4p, so that dipole transitions of the type $[\mathrm{Ne}]3l^2 4p \rightarrow [\mathrm{Ne}]3l^2 5s$ are energetically allowed even though $\langle E\rangle_{[\mathrm{Ne}](3)^2(5)^1} > \langle E\rangle_{[\mathrm{Ne}](3)^2(4)^1}$ As long as these "inverted" rates are small compared to both the total rate out of the lower-energy SC and the "normal" rates coupling the SCs, they can be safely neglected. For inverted rates among excited SCs, ΔE^2 scaling tends to ensure that radiative decay rates to the ground SC dominate over the inverted rates, so the first criterion is typically met. And a rough scaling of radiative to collisional rates among ground and excited states suggests that as long as the typical transition energy of the inverted decay rates is much less than the typical energy of the excited SCs from the ground SC, the electron density will be either so high that the "normal" collisional excitation rate dominates over the inverted decay rate or so low that the ground SC dominates the population flux, or both. However, since this criterion is least likely to hold for near-neutral ions, the very ions for which the orbital binding energies are most likely to be disordered, screened hydrogenic models ought to be used with caution at low temperatures.

Including inverted radiative decay transitions *from* ground SCs (for example, the 3d→4s decay in neutral potassium, whose ground SC is $[\mathrm{Ne}](3)^9$ but whose ground configuration is $[\mathrm{Ne}]3s^2 3p^6 4s$) is wholly inadvisable, since at sufficiently low densities it can lead to populations in the excited $[\mathrm{Ne}](3)^8(4)^1$ SC that are much larger than could be supported by collisional excitation, leading, for example, to radiative loss rates that are orders of magnitude too

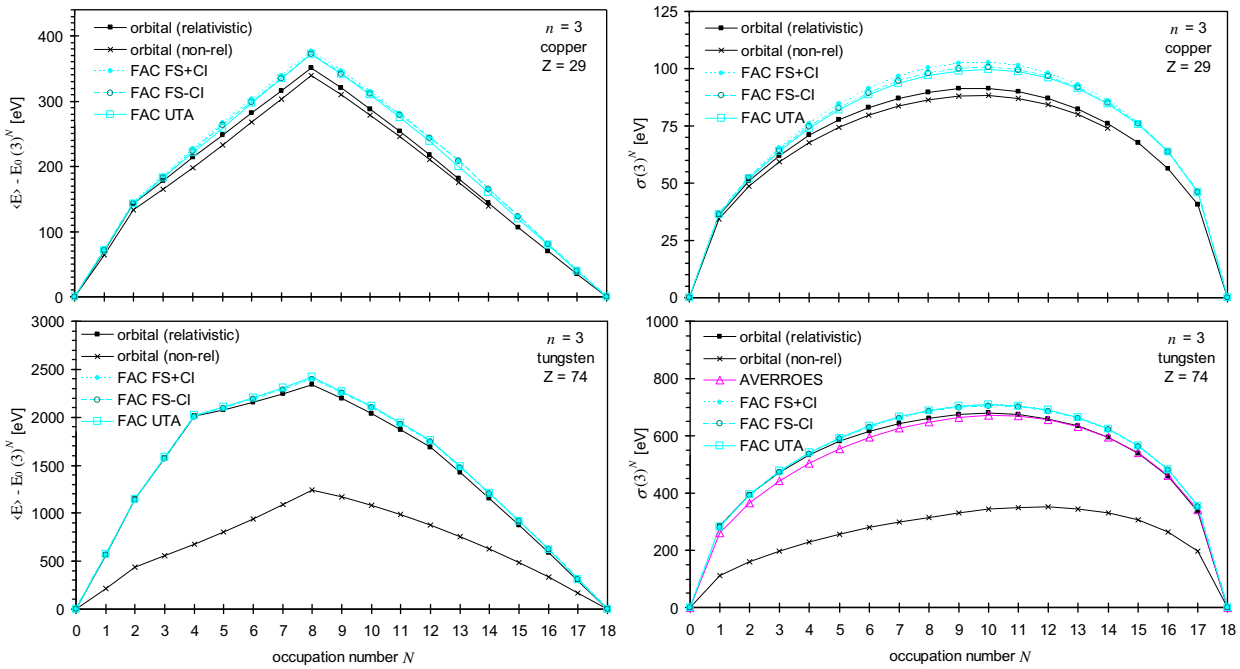

Fig. 3. As in Fig. 2 for the M-shells of copper and tungsten.

large (see the similar problem arising from a direct configuration averaging of fine structure states in highly charged W discussed in Ref. [42]).

Since inverted rates of radiative recombination and collisional ionization should follow scaling similar to that of radiative decay and collisional excitation, it seems acceptable to exclude from the rate matrix any single-electron process that is not energetically allowed, just as if the SCs had zero energy widths.

The arguments above provide some justification for the standard approach taken by screened hydrogenic models that treat SCs

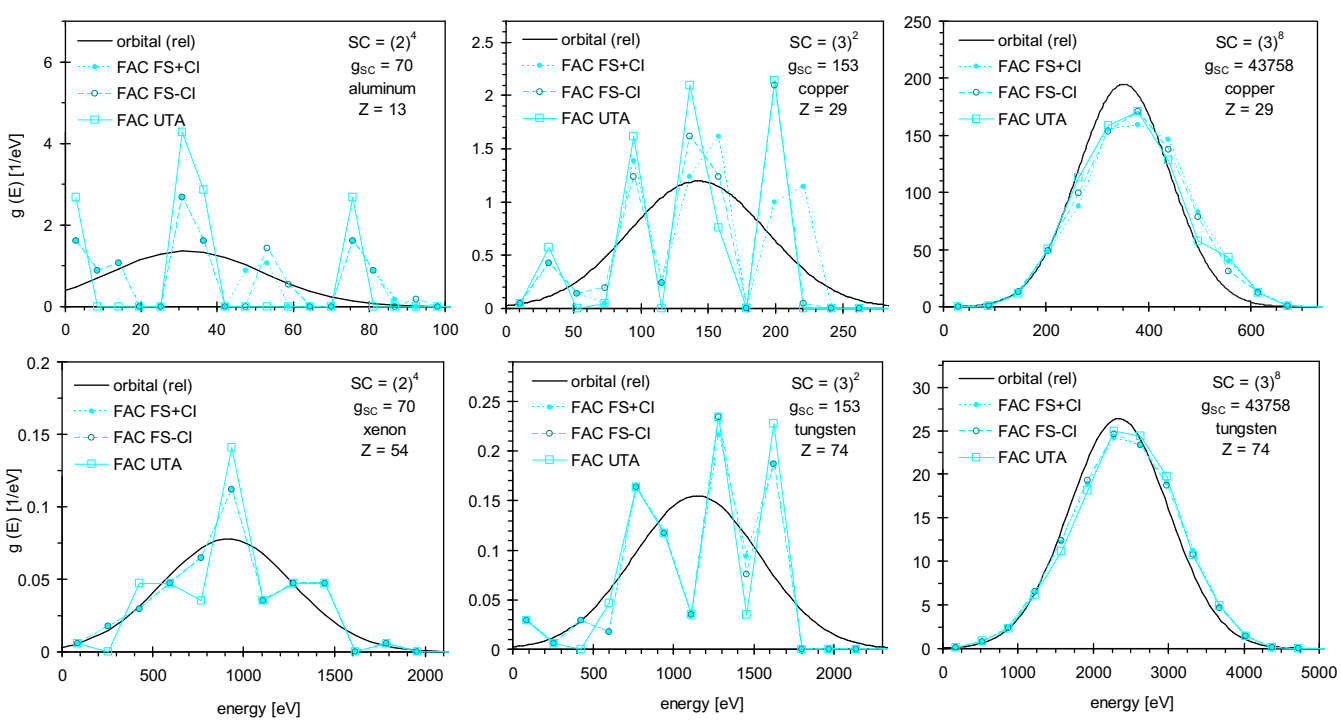

Fig. 4. Distributions of level statistical weights g as a function of level energy E. Results from the detailed atomic structure code FAC (cyan) are compared with distributions based on the approximate orbital expressions for various L- and M-shell ions.

Please cite this article in press as: S.B. Hansen, et al., Superconfiguration widths and their effects on atomic models, High Energy Density Physics (2010), doi:10.1016/j.hedp.2010.07.002

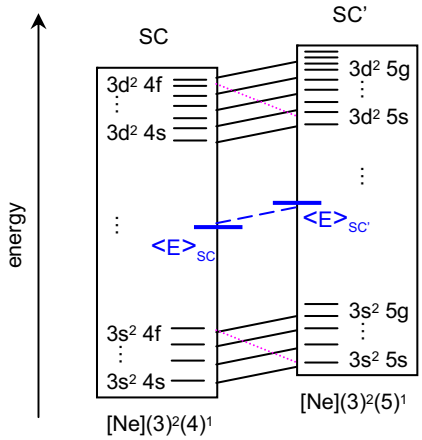

Fig. 5. Schematic of the first two excited superconfigurations in neutral aluminum and the rates between them.

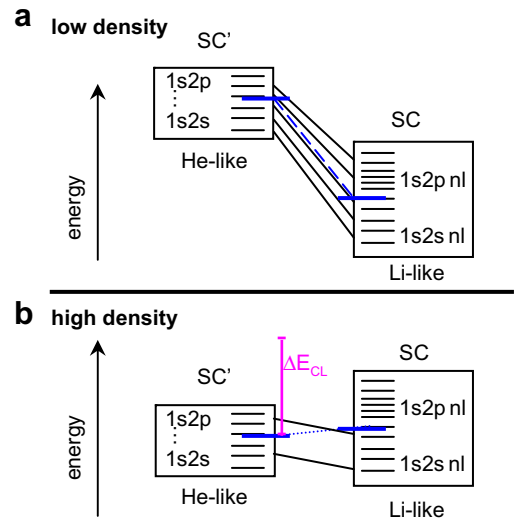

Fig. 6. Schematic of the He- and Li-like excited SCs at low (a) and high (b) density. Continuum lowering changes the relative average energies of configurations in neighboring ions and can prematurely destroy important ionization channels in zero-width SC models.

as though they have negligible energy widths and compute all rates based on differences of average SC energies and total statistical weights. However, even in the absence of inverted rates, this justification breaks down in at least three cases: (1) strong continuum lowering that changes the relative energies of SCs in neighboring ions so that an energetically allowed transition becomes forbidden, even when rates between sublevels persist; (2) dielectronic recombination, where part of an SC lies above the continuum limit even though the average SC energy lies below it; and (3) "hybrid-structure" atomic models, where rates from high-lying SCs are coupled to more detailed levels with much smaller (or zero) statistical widths. Below, we discuss each of these cases in turn.

3.1. Continuum lowering

To illustrate the effects of continuum lowering on rates between SCs in screened hydrogenic models, Fig. 6 gives an energy level schematic of He- and Li-like ions at low and high densities. At the low density, the whole of the Li-like $(1)^1(2)^1(n)^1$ superconfiguration lies below the average energy of the He-like $(1)^1(2)^1$ SC and each Li-like level can ionize to one in the He-like SC by losing its n-shell electron. At the higher density, the continuum lowering that has shifted the continuum limits of the two ions by $E_{\mathrm{CL}} = 3/2(Z_{\mathrm{ion}}+1)[3/(4\pi n_{\mathrm{ion}})]^{1/3}$[Hartrees] [43] has also shifted their relative energies by ΔE_{CL}, so that the average energy of the Li-like SC is above that of the He-like SC. If the absolute value of the energy difference between the central energies of the two SCs remains less than the standard deviation of the n shell (which controls the destruction of the outer orbital by pressure ionization), then the collisional ionization rate will vanish in a zero-width SC model even though ionization is energetically allowed for the more tightly bound of the Li-like nl orbitals. (For example, in a configuration model, 1s 2p 5s exists and can ionize to 1s 2p even after 1s 2p 5f is pressure ionized.) Further, just before the coupling rates vanish in a zero-width SC model, they become very strong as the density increases and the energy difference decreases. Even if one employs a statistical reduction factor on the outer orbitals as described in Ref. [44], some portion of the SC persists after the average energies cross. Thus, to prevent unphysical oscillations and discontinuities in the SC populations as n-shells are progressively pressure-ionized, the ionization rates must be continuously modified as E_{CL} increases, ideally in such a way that the low-density limit preserves the zero-width rates and the rates decline smoothly to vanish when the negative of the transition energy exceeds the standard deviation of the n-shell orbitals. One candidate for such a modification is the prefactor

$$f_{\mathrm{ion}} = 1 - \frac{E_{\mathrm{CL}}}{\left|E_n^{\mathrm{b}}\right| + \sigma_n} \tag{12}$$

Here, E_n^{b} is the binding energy of the n-shell in the isolated ion limit and σ_n is its standard deviation. Applying this prefactor (or something like it designed to join with a statistical reduction factor) to collisional and photoionization processes as well as their reverse rates ensure that the SC populations vary smoothly with density.

3.2. Dielectronic recombination

The arguments given in the first part of this section to justify the zero-width SC approximation apply only to SCs between which inverted rates are negligible. For single-electron transitions among the excited states of highly charged ions, this condition is met naturally. By contrast, inverted two-electron process of dielectronic capture (d.c.) can be a dominant component of the total rate leaving a ground-state SC, particularly at low electron densities where radiative and three-body recombination and collisional excitation from the ground states are small. Fig. 1 illustrates a case in which autoionization in zero-width SC models may be improperly treated: the high-n $(1)^2(2)^8(3)^5(n)^1$ SCs, which are singly excited in the SC notation, contain multiply excited configurations that can autoionize even though their central energies lie below that of the $(1)^2(2)^8(3)^5$ SC. (These are the $\Delta n = 0$ transitions that can dominate the dielectronic recombination rate at low temperatures). Even SCs that are doubly excited in the SC notation can be inverted, for example, the SC $(1)^2(2)^8(3)^6(4)^2$ in Ar-like tungsten has an energy that lies below $(1)^2(2)^8(3)^7$ by about half its standard deviation. Such SCs would not be properly coupled in a zero-width SC model, and this can be significant since the low-n Auger transitions most likely to be inverted tend to be strong channels due to the $1/n^3$ scaling of Auger rates. To improve the treatment of two-electron

processes in screened hydrogenic SC models, we propose including all possible dielectronic capture transitions weighted by the fraction of the statistical weight above the ionization limit in the autoionizing SC:

$$f_{dc} = \frac{1}{g_{SC}} \int_{E_a}^{\infty} g(E)\, dE = \frac{1}{2}\left[1 - \mathrm{erf}\left(\frac{\Delta E_{dc}}{\sqrt{2}\sigma}\right)\right] \tag{13}$$

Here, erf is the error function and ΔE_{dc} is the energy difference between the initial and final SCs in the autoionization process: $\Delta E_{\mathrm{dc}} = IP^{Z,\ Z+1} + E_f^{Z+1} - E_i^{Z}$ (where E_f^{Z+1} and E_i^{Z} are the average SC energies of the ionized and autoionizing SC, respectively, relative to the average energy of the ground SCs in each ion), and the lower limit of the integral $E_{\mathrm{a}} = IP^{Z,\ Z+1} + E_f^{Z+1}$. In the limit of the normal autoionization process, ΔE_{dc} is negative and f_{dc} goes to unity. For inverted processes, f_{dc} lies between zero and 1/2. The fraction adjusts smoothly under continuum lowering as the ionization potential $IP^{Z,\ Z+1}$ is modified. At plasma conditions where the auotionizing states are nearly statistically populated or where dielectronic capture is the dominant rate into the auotionizing SC, this factor can also be applied directly to the Auger rates so that detailed balance is preserved. However, for SCs that are populated dominantly through direct collisional excitation whose population at low temperatures is concentrated in the lowest-energy members of an ensemble, the factor f_{dc} can significantly overestimate the actual flux through excitation-autoionization channels. We thus propose a modified expression for $\Delta n = 0$ autoionization rates that folds a Boltzmann factor into Eq. (13):

$$\begin{aligned} f_{Aug}^{\Delta n=0} &= \tfrac{1}{g_{SC}} \int_{E_a}^{\infty} g(E) e^{-(E-E_0)/T_e}\, dE \\ &= \tfrac{1}{2} e^{\left(\sigma^2/2T_e^2 - (\langle E\rangle - E_0)/T_e\right)} \left[1 - \mathrm{erf}\left(\frac{\sigma^2 + \Delta E_{dc} T_e}{\sqrt{2}\sigma T_e}\right)\right] \end{aligned} \tag{14}$$

Here, E_0 is the energy of the lowest-lying configuration in the autoionizing SC, so that $(\langle E\rangle - E_0)$ is the relative average SC energy as plotted in Figs. 2 and 3. In the high-temperature limit, $f_{\mathrm{Aug}} \to f_{\mathrm{dc}}$.

Non-Maxwellian or beam plasmas are another case in which the width of autoionizing SCs becomes important. In an electron beam ion trap (EBIT), the beam electrons that govern excitation, ionization, and recombination can have a full width at half max as small as $\approx$20 eV – much smaller than the standard deviations of the SCs in many mid-shell ions. The resonant dielectronic capture cross section is treated as a delta function and its intersection with the finite-width beam determines the capture rate. If the autoionizing states are densely populated, the narrow beam moves into and out of resonance with different fine structure states more or less smoothly as the beam energy changes. But in a zero-width SC model, autoionizing states sparsely populate the continuum and any resonance with the narrow beam is fortuitous. To mimic a densely modeled continuum using SCs in cases where the standard deviation of the capture process σ_{dc} is larger than that of the beam energy, one can use the $g(E)$ given in Eq. (11) rather than a delta function for the dielectronic capture cross section.

The variance σ_{dc}^2 for the dielectronic capture and autoionization processes is in principle that of the strength-weighted *emissive zone* of the autoionizing SC, rather than simply the variance of the SC σ_{SC}^2. However, in contrast with the emissive zones defined for transition arrays between configurations [45], σ_{dc}^2 does not differ much from the variances of the involved SCs, because it depends essentially on the average upper energies of the superarrays, and very little on their separate widths. Calculations of the emissive zones of the superarrays are given in the Appendix.

3.3. Supplementing hybrid-structure models with superconfigurations

The strength of screened hydrogenic SC models is in their compact completeness. They can provide reasonably reliable predictions for the gross properties (charge state distribution, radiative power loss rates) of even complex mid-shell ions. And it is relatively simple to extend their structure to include higher n-shells, deeper holes, or multiple excitations in order to verify model completeness and to modify the rate approximations in order to test model sensitivity to various processes. However, SC models cannot generally produce spectroscopic-quality emission or absorption data, even when coupled with more sophisticated transition data as in Ref. [3]. Apart from intensive efforts to provide benchmark calculations (*e.g.* the carbon models described in Ref. [46]), the fine-structure models that *can* generate high-quality non-LTE spectra are generally limited by computational constraints to relatively simple ions near closed shells or to low-density coronal conditions where only single excitations from the ground configuration are important, and where all dielectronic capture and decay channels that involve multiply excited states can be represented by a single dielectronic recombination rate (as done in Refs. [47,48]).

A hybrid-structure model that captures the advantages of both screened hydrogenic SC and fine structure models has been described in Refs [28,29]. In this approach, a small set of singly excited "coronal" levels (including single excitations from inner shells) and the rates coupling them are computed in fine structure detail. These are combined with a larger set of relativistic configurations and UTA rates that includes all of the coronal configurations as well as additional singly and multiply excited states. Typical configuration-interaction effects on transition energies and rates (*c.f.* [49,50]) are determined by comparing the overlapping set of fine-structure and UTA transitions, and these effects are extended to all transitions in the hybrid-structure model. Finally, supplementally screened hydrogenic SCs are folded into the mix in order to ensure completeness with the same ease as in a pure SC model.

In our implementation of the hybrid-structure scheme, a data set of mixed fine-structure and UTA states and rates for all ions of an element is generated and stored in large data files. To find populations and spectra for a given set of plasma conditions, a pure screened hydrogenic SC model is generated on-the-fly to provide an initial estimate for the average ion charge. This average ion charge is then used to set a window within which the detailed states are mixed with supplemental SCs and beyond which a pure SC representation is retained. The mixing of detailed and SC states can generally proceed under the zero-width approximation, as long as the modifications described above have been included in generating the SC-model structure and rates. However, energy differences between SCs can no longer be treated as being the differences between their central (average) energies. Instead, they must be treated as if they represent the energy differences between the lowest-energy members of the SC ensemble. Thus, an excitation rate that in a pure SC model took place from some average state in the lower SC to some average state in the upper SC is now imagined to be a process between the lowest-energy members of the SCs. This shift in representation is necessary because the ground-state levels of the hybrid-structure ions are no longer large ensembles but are true ground states.

This shift is schematically illustrated in Fig. 7. It permits us to continue to use directly all of the energies and rates that were determined in the pure SC model if the rates from SCs to detailed levels i are modified by a simple Boltzmann factor:

$$R(\mathrm{SC} \to i' \in \mathrm{SC}') = \frac{g_{i'}}{g_{SC'}} e^{-(E_{i'} - E_{SC'})/T_e} R(\mathrm{SC} \to \mathrm{SC}') \tag{15}$$

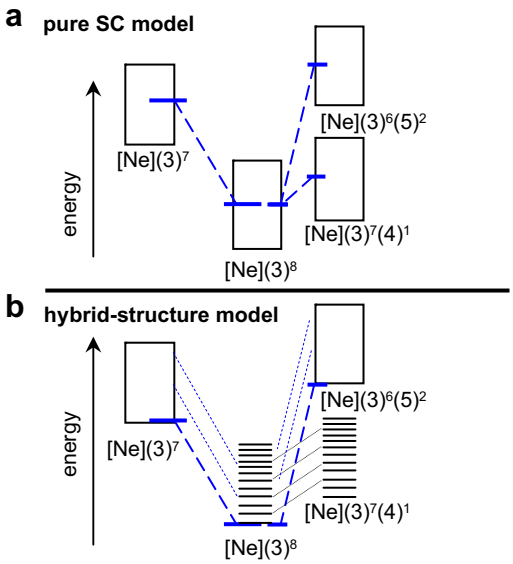

Fig. 7. Energy differences between average SC energies (a) are shifted to represent energy differences between the lowest-energy members of the SCs (b) for use in hybrid-structure models that contain true ground states.

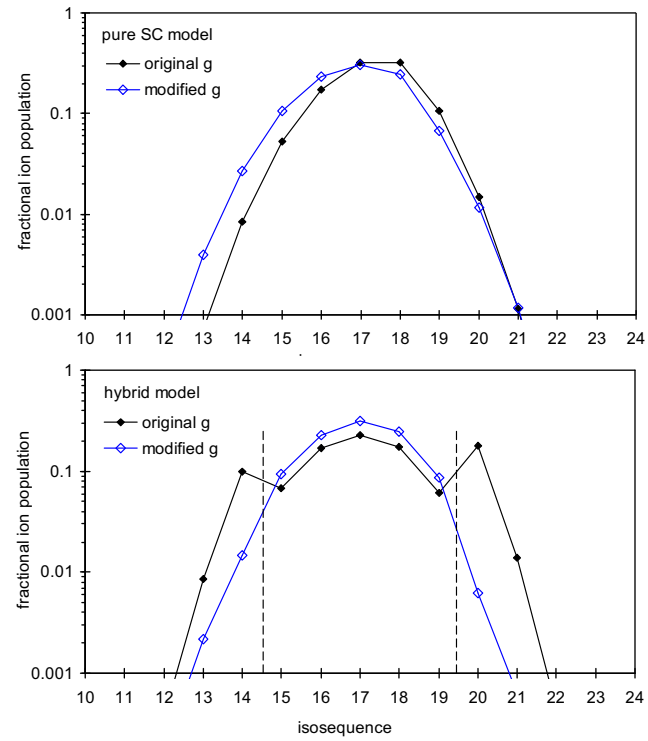

Fig. 8. Modifying the statistical weights of SCs to account for internal partition functions in copper ($\rho = 8$ g/cm^3; $T_e = 100$ eV) changes the calculated charge state distributions for both a pure SC model (top) and a hybrid-structure model (bottom) that uses pure SCs for ions outside the window indicated by the vertical dashed lines.

Here, E'_{SC} is the energy of the final SC relative to the ground SC of that ion. The reverse rates $R(i \in SC \rightarrow SC')$ represent an average from any level in the initial SC to the whole of the final SC′ and so remain unchanged. Compared with statistical factors based on the Gaussian distributions, the Boltzmann factor here is a rough approximation. But it is enough to ensure that the hybrid-model populations approach their LTE limit at high densities or when the radiation temperature equals the electron temperature T_e. An effective temperature [23,51] in place of T_e may improve the approximation, but this has not been extensively studied.

In considering the boundaries of the ion window described above, within which ions have hybrid structure and outside of which ions are pure SCs, it becomes apparent that an additional modification must be made to all of the SC states in order to ensure model coherence. If the SC-to-hybrid boundary occurs between, for example, the Si-like ion with 14 electrons and the P-like ion with 15 electrons, then the model will have a ground SC $(3)^4$ with a statistical weight of more than 3000 adjacent to a ground level $3p^3(J = 3/2)$ with a statistical weight of 4. Even at high densities, where the partition function spreads population throughout the ground SC of the hybrid-structure ion, this imbalance can lead to discontinuities in the charge state distribution like the one illustrated in the lower panel of Fig. 8 for near-solid copper at $T = 100$ eV. We thus propose that in the hybrid model, the statistical weights of the SCs be modified to reflect an internal population distribution that follows Boltzmann statistics:

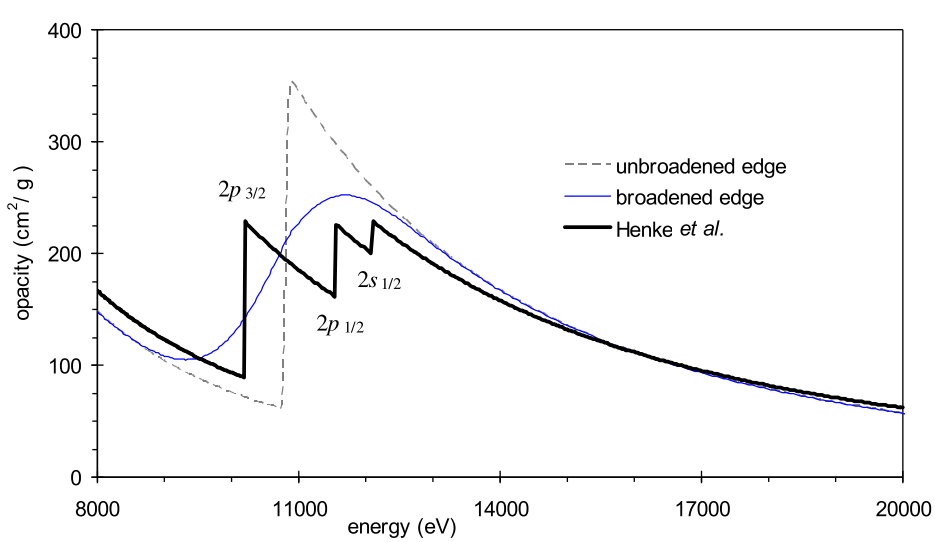

Fig. 9. The SC variances can be used to give reasonable widths to bound-free edges in screened hydrogenic models, illustrated here for the L-edge of cold tungsten.

Please cite this article in press as: S.B. Hansen, et al., Superconfiguration widths and their effects on atomic models, High Energy Density Physics (2010), doi:10.1016/j.hedp.2010.07.002

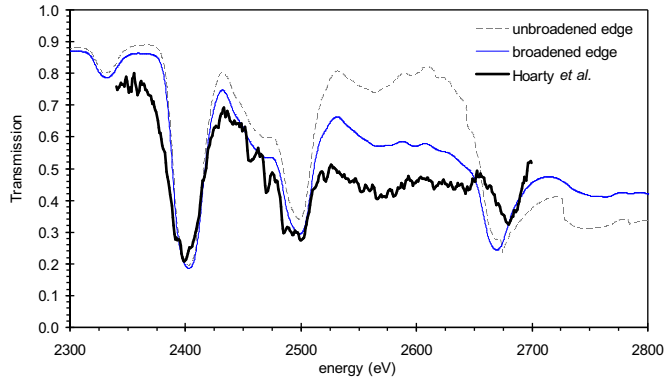

Fig. 10. Broadening the bound-free edges according to the estimated SC variances improves the agreement between a screened hydrogenic model with LIMBO nlj–$(nlj)'$ transitions (shifted by 50 eV to agree with more detailed calculations) and the measured transmission of niobium at $T = 30$ eV and $\rho = 0.028$ g/cm^3 from Ref. [53].

$$g_{\mathrm{SC}}^{\mathrm{mod}} = \int_{E_0}^{\infty} g(E) e^{-(E-E_0)/T_{\mathrm{e}}}\, \mathrm{d}E = \frac{g_{\mathrm{SC}}}{2} e^{\left(\sigma^2/2T_{\mathrm{e}}^2 - (\langle E\rangle - E_0)/T_{\mathrm{e}}\right)} \left[1 - \mathrm{erf}\left(\frac{\sigma^2 - T_{\mathrm{e}}E_0}{\sqrt{2}\sigma T_{\mathrm{e}}}\right)\right] \tag{16}$$

with E_0 the energy of the lowest-lying configuration in the SC, as in Eq. (14).

All of the $R(\mathrm{SC}\rightarrow\mathrm{SC}')$ rates can be modified by the factor $g_{\mathrm{SC}'}^{\mathrm{mod}}/g_{\mathrm{SC}'}$ to reflect the modified partition function in the final SC. Modified statistical weights can be computed for each SC individually, or the ratio of the ground SC for each ion can be used to set a single reduction factor for each ion in order to preserve the pure-SC model rates within the ions. The SC energies can also be changed from $\langle E\rangle$ to $\langle E\rangle - \sigma^2/T_{\mathrm{e}}$, which is the energy at which $g(E)e^{-(E-E_0)/T_{\mathrm{e}}}$ reaches its maximum. The effects of using modified statistical weights for the SCs are illustrated in Fig. 8. The top panel shows that reducing the statistical weights for each SC according to Eq. (16) shifts the ionization balance slightly away from the high-g mid-shell ions. The bottom panel shows the results from a hybrid-structure model with a narrow window for the more detailed ions: without the reduction of g_{SC}, there is a discontinuity at the SC-to-hybrid-structure boundaries, which is corrected when g_{SC} are modified.

So far, we have only used the electron temperature (or beam energy, for EBIT sources) to determine the internal partition function and have found this to give reasonably smooth charge state distributions at a variety of plasma conditions. However, effective temperatures such as those determined by the MOST model [23,24] might increase the accuracy of the hybrid model further and are currently being investigated along with effective temperatures in the rate modification factors of Eq. (15).

4. Effects of SC widths on bound-free spectra

As mentioned above, the most obvious failure of pure SC models is the lack of structure apparent in their computed spectra. While the SC variances presented here could in principal be used to estimate the widths of SC-to-SC transition arrays, a much better approach to calculations of bound-bound spectra is to use tabulated energies and strengths for nl–$(nl)'$ or nlj–$(nlj)'$, as done in, for example, Ref. [3]. In the present SC model, internal SC partition functions and approximate UTA widths are folded into the nlj–$(nlj)'$ transitions and, where more detailed transition data is at hand (e.g. from hybrid-structure levels), transition energies are adjusted to give better accuracy. A similar splitting could be included for bound-free edges in pure SC models, but we have found that broadening the bound-free edges by $\sigma_{\mathrm{edge}}^2 = \sigma_{\mathrm{SC}_i^Z}^2 + \sigma_{\mathrm{SC}_f^{Z+1}}^2$ gives reasonable results. Fig. 9 illustrates such broadening for the L-shell absorption edge of cold tungsten, compared with the nlj – split cold opacity from Henke [52]. The 1.4–2 keV energy difference between the $j = 1/2$ and $j = 3/2$ orbitals is significantly larger than the energy differences between adjacent ions, and the SC model with a broadened edge is in much better agreement with the more detailed data. Fig. 10 illustrates that this edge broadening also improves agreement with the absorption spectrum measured recently by Hoarty et al. [53], which captures $n = 2$ to $n = 4$ transitions and the L-edges of niobium ionized to the N-shell.

5. Summary

We have presented several expressions to compute average energies and energy variances of superconfigurations from one-electron orbitals and have found our approximations to be in reasonable agreement with more sophisticated calculations. Using the presented approximations to generate distributions of energy levels within SCs allows us to refine the standard zero-width treatment of SCs in the screened-hydrogenic models that are widely and successfully used for non-LTE calculations. These refinements are particularly important for improving accuracy in continuum lowering and dielectronic capture in pure SC models. Although the suggested refinements are rather crude corrections in comparison to more sophisticated treatments of correlations between superconfigurations based on explicit internal SC structure [23,24], they have a useful function as rough but reasonable corrections to a rough but reasonable class of atomic models. Finally, we have shown that the energy variances of superconfigurations also play an important role in the construction of reliable and computationally tractable hybrid-structure atomic models that can generate highly accurate equations of state and radiative properties for ions of arbitrary complexity.

Acknowledgements

We thank Brian Wilson and Olivier Peyrusse for providing, respectively, the LIMBO and AVERROES data used in this study. We are grateful to David Hoarty for providing the experimental niobium transmission spectrum, to Howard Scott, Hyun-Kung Chung, and Mark May for helpful conversations on screened hydrogenic models and dielectronic recombination, and to the anonymous reviewers of this paper who helped clarify the presentation. Sandia is a multiprogram laboratory operated by Sandia Corporation, a Lockheed Martin Company, for the United States Department of Energy under contract DE-AC04-94AL85000.

Appendix A. Computation of emissive zones for the rate calculations

Superconfigurations (SCs) are useful for non-LTE plasma calculations because of their compactness and the relatively simple global approximations available for rates between SCs. However, such global approximations generally do not take into account several important corrections. In Section 3, we have proposed corrections related to overlapping SCs for autoionization and dielectronic capture rates and for other ionization processes in the presence of strong continuum lowering, and have argued that no such corrections are required for monoelectronic processes in the absence of continuum lowering due to the propensity correlation [24,41].

And we have given in Eq. (16) an expression that modifies the statistical weights of the SC (and through them, the rates) to reflect an internal partition function that changes with the plasma conditions (this is equivalent to shifting the central energies of $g(E)$ via multiplication by a Boltzmann factor). However, the proposed corrections were derived with the assumption that the strengths of the processes between different components of the SCs are equally weighted. In this appendix, we demonstrate that this is not the case, in general, and give quantitative examples to guide future corrections to approximate SC-to-SC rates.

For the evaluation of global rates between SCs, it is interesting to take into account the contributions of the levels with the larger strengths, *i.e.*, the levels of the *emissive zones* of the upper SC [45] (see Section 3.2).

Taking $(3)^N(4)^1 \rightarrow (3)^{N+1}$ as a typical case, the quantity

$$\mu_n\left((3)^N(4)^1\right) = \sum_{i,j} E(C_i)^n S(C_i \rightarrow C_j)/S_{\text{tot}} \tag{17}$$

is the statistical moment of order n of the emissive zone of $(3)^N(4)^1$. In Eq. (17), the sums over i and j run over all the configurations of $(3)^N(4)^1$ and $(3)^N$, respectively, $E(C_i)$ is the energy of C_i, $S(C_i \rightarrow C_j)$ is the electric-dipolar strength of the transition array $C_i \rightarrow C_j$, and S_{tot} is the sum of all such strengths. In this global approach, $E(C_i)$ is the average energy of C_i, represented as a sum of monoelectronic quantities, denoted E_{nl}. For example,

$$\begin{aligned} E\left(3s^\alpha 3p^\beta 3d^\gamma 4f\right) &= \alpha E_{3s} + \beta E_{3p} + \gamma E_{3d} + E_{4f} \\ &= \alpha S + \beta P + \gamma D + F' \end{aligned} \tag{18}$$

in simpler notation. Instead of computing explicitly Eq. (17) for each value of N, it is very convenient to use the laws of complementarity and anticomplementarity between the *centered* moments $\mu_n^c((3)^N(4)^1)$ and $\mu_n^c((3)^{17-N}(4)^1)$:

$$\mu_{2k}^c\left((3)^N(4)^1\right) = \mu_{2k}^c\left((3)^{17-N}(4)^1\right) \tag{19}$$

$$\mu_{2k+1}^c\left((3)^N(4)^1\right) = -\mu_{2k+1}^c\left((3)^{17-N}(4)^1\right) \tag{20}$$

where k is a positive integer. These laws are valid for the entire $(3)^N(4)^1 \rightarrow (3)^{N+1}$ emission, because they can be proved for each of its $4l \rightarrow 3l'$ supertransition arrays, *e.g.*, $4d \rightarrow 3p$ for $N = 2$ and 15:

$N=2$ array	Total strength	Upper energy E_u	E_u for $S=1$, $P=2$, $D=4$
$3s^2 4d \rightarrow 3s^2 3p$	$4P^2 \times 1$	$E_{4d} + 2S$	$E_{4d} + 2$
$3s3p4d \rightarrow 3s3p^2$	$4P^2 \times 10$	$E_{4d} + S + P$	$E_{4d} + 3$
$3s3d4d \rightarrow 3s3p3d$	$4P^2 \times 20$	$E_{4d} + S + D$	$E_{4d} + 5$
$3p^2 4d \rightarrow 3p^3$	$4P^2 \times 10$	$E_{4d} + 2P$	$E_{4d} + 4$
$3p3d4d \rightarrow 3p^2 3d$	$4P^2 \times 50$	$E_{4d} + P + D$	$E_{4d} + 6$
$3d^2 4d \rightarrow 3d^2 3p$	$4P^2 \times 45$	$E_{4d} + 2D$	$E_{4d} + 8$
	Total $4P^2 \times 136$		
$N=15$ array	Total strength	Upper energy E_u	E_u for $S=1$, $P=2$, $D=4$
$3p^5 3d^{10} 4d \rightarrow 3p^6 3d^{10}$	$4P^2 \times 1$	$E_{4d} + 5P + 10D$	$E_{4d} + 50$
$3s3p^4 3d^{10} 4d \rightarrow 3s3p^5 3d^{10}$	$4P^2 \times 10$	$E_{4d} + S + 4P + 10D$	$E_{4d} + 49$
$3s3p^5 3d^9 4d \rightarrow 3s3p^6 3d^9$	$4P^2 \times 20$	$E_{4d} + S + 5P + 9D$	$E_{4d} + 47$
$3s^2 3p^3 3d^{10} 4d \rightarrow 3s^2 3p^4 3d^{10}$	$4P^2 \times 10$	$E_{4d} + 2S + 3P + 10D$	$E_{4d} + 48$
$3s^2 3p^4 3d^9 4d \rightarrow 3s^2 3p^5 3d^9$	$4P^2 \times 50$	$E_{4d} + 2S + 4P + 9D$	$E_{4d} + 46$
$3s^2 3p^5 3d^8 4d \rightarrow 3s^2 3p^6 3d^8$	$4P^2 \times 45$	$E_{4d} + 2S + 5P + 8D$	$E_{4d} + 44$
	Total $4P^2 \times 136$		

Note that the numerical values chosen above for the S, P, and D quantities are arbitrary, which makes the numerical proof a general proof.

In each of the corresponding 6 lines of these tables, the strengths are the same, and the sum of the two E_u quantities is equal to $2E_{4d} + 52$. The quantity $2E_{4d}$ disappears in the calculation of centered moments. From these results, we can deduce Eqs. (19) and (20).

From the complementarity or anticomplementarity properties, equations can be derived for the centered moments $\mu^c{}_2$, $\mu^c{}_3$, and $\mu^c{}_4$, which are the most interesting for the description of a statistical distribution. The N-dependences of these moments are contained in the following equations:

$$\begin{aligned} \mu_2^c(N) &= AN(17-N) + B \\ \mu_3^c(N) &= (2N-17)\left[A'\left(2N^2 - 34N - 289\right) + B'\right] \\ \mu_4^c(N) &= N(N-17)\left[A'\left(N^2 - 17N - 289\right) + B''\right] + C'' \end{aligned} \tag{21}$$

where the coefficients A–C'' are functions of S, P, and D. Moreover, the sum $[\mu_1(N) + \mu_1(17-N)]$ does not depend on N.

Since B can be found to vanish (computing explicitly $\mu_2{}^c(N)$ for $N = 1$ and 2), the variances $\mu_2{}^c$ of the emissive zones of the superarrays belonging to $(3)^N(4)^1 \rightarrow (3)^{N+1}$ are given by Eq. (21) with the following values for the coefficient A:

$$\begin{aligned} A(4s \rightarrow 3p) &= \left(15S^2 + 30P^2 + 35D^2 - 10SP - 20SD - 50PD\right)/2312 \\ A(4p \rightarrow 3s) &= \left(8S^2 + 33P^2 + 35D^2 - 6SP - 10SD - 60PD\right)/2312 \\ A(4p \rightarrow 3d) &= \left(15S^2 + 33P^2 + 36D^2 - 12SP - 18SD - 54PD\right)/2312 \end{aligned} \tag{22}$$

Moreover, the coefficients for $4d \rightarrow 3p$ and $4f \rightarrow 3d$ are the same as for $4s \rightarrow 3p$ and $4p \rightarrow 3d$, respectively.

The average energies of the emissive zones in the superarrays belonging to $(3)^N(4)^1 \rightarrow (3)^{N+1}$ are:

$$\begin{aligned} \mu_1(4s \rightarrow 3p) &= E_{4s} + N(2S + 5P + 10D)/17 \\ \mu_1(4p \rightarrow 3s) &= E_{4p} + N(S + 6P + 10D)/17 \\ \mu_1(4p \rightarrow 3d) &= E_{4p} + N(2S + 6P + 9D)/17 \\ \mu_1(4d \rightarrow 3p) &= E_{4d} + N(2S + 5P + 10D)/17 \\ \mu_1(4f \rightarrow 3d) &= E_{4f} + N(2S + 6P + 9D)/17 \end{aligned} \tag{23}$$

The average energy of the *total* emissive zone of the upper SC is deduced from the average energies and strengths of its superarrays.

$$\begin{aligned} \mu_1\left((3)^N(4)^1\right) = \Big[&2P(4s \rightarrow 3p)^2 \mu_1(4s \rightarrow 3p) \\ &+ 2P(4p \rightarrow 3s)^2 \mu_1(4p \rightarrow 3s) \\ &+ 4P(4p \rightarrow 3d)^2 \mu_1(4p \rightarrow 3d) \\ &+ 4P(4d \rightarrow 3p)^2 \mu_1(4d \rightarrow 3p) \\ &+ 6P(4f \rightarrow 3d)^2 \mu_1(4f \rightarrow 3d)\Big]/S_{\text{tot}} \end{aligned} \tag{24}$$

where S_{tot} is the total strength:

$$\begin{aligned} S_{\text{tot}} = {}& 2P(4s \rightarrow 3p)^2 + 2P(4p \rightarrow 3s)^2 + 4P(4p \rightarrow 3d)^2 \\ &+ 4P(4d \rightarrow 3p)^2 + 6P(4f \rightarrow 3d)^2 \end{aligned} \tag{25}$$

Because Eq. (21) is fulfilled by all the 5 superarrays, the variance of the emissive zone of the upper SC fulfills the same equation. It contains the A quantities of the superarrays, their average energies μ_1, and their total strengths S.

$$\begin{aligned} \mu_2^c\left((3)^N(4)^1\right) = {}& \sum_{i=1,5} S(i)\left[\mu_2^c(i) + \mu_1^2(i)\right]/S_{\text{tot}} \\ &- \left[\sum_{i=1,5} S(i)\mu_1(i)/S_{\text{tot}}\right]^2 \end{aligned} \tag{26}$$

Please cite this article in press as: S.B. Hansen, et al., Superconfiguration widths and their effects on atomic models, High Energy Density Physics (2010), doi:10.1016/j.hedp.2010.07.002

where the sums run over the 5 superarrays. The strengths $S(i)$ are the 5 terms at the right of Eq. (25).

The above results relate to the E1 emission process. However, they can also be used for the autoionization (*ai*) and resonant capture (*rc*) processes, due to two correlations (see Ref. [24]).

(i) First correlation. The correlation between the energies of the configurations of the two SCs is asserted, because it relies on the fact that the spectator electrons ought to be the same in both SCs. The number of these electrons is smaller by one in the *ai* process, but this is a small difference.
(ii) Second correlation. Although the diversity of autoionization and resonant-capture rates cannot be evaluated simply, these rates nearly obey approximate linear variations vs configuration energies in $(3)^N(4)^1$.

References

[1] W.A. Lokke, W.H. Grasberger, UCRL-52276. Lawrence Livermore National Laboratory, Livermore, CA, 1977.
[2] H.-K. Chung, M.H. Chen, W.L. Morgan, Y. Ralchenko, R.W. Lee, High Energy Dens. Phys. 1 (2005) 3.
[3] H. Scott, S.B. Hansen, High Energy Dens. Phys. 6 (2010) 39.
[4] A. Bar-Shalom, M. Klapisch, J. Oreg, J. Quant. Spectrosc. Radiat. Transf. 71 (2001) 169.
[5] M.F. Gu, Astrophys. J. 582 (2003) 1241.
[6] D.H. Sampson, H.L. Zhang, C.J. Fontes, Phys. Rep. 477 (2009) 111.
[7] M.Ya. Amusia, L.V. Chernysheva, Computation of Atomic Processes: A Handbook for ATOM programs. IOP, 1997.
[8] R.W. Lee, J.K. Nash, Y. Ralchenko, J. Quant, Spectrosc. Radiat. Transf. 58 (1997) 737.
[9] C. Bowen, A. Decoster, C.J. Fontes, K.B. Fournier, O. Peyrusse, YuRalchenko, J. Quant. Spectrosc. Radiat. Transf. 81 (2003) 71.
[10] C. Bowen, R.W. Lee, YuRalchenko, J. Quant. Spectrosc. Radiat. Transf. 99 (2006) 102.
[11] J. Rubiano, R. Florido, C. Bowen, R. Lee, YuRalchenko, High Energy Dens. Phys. 3 (2007) 225.
[12] C.J. Fontes, J. Abdallah Jr., C. Bowen, R.W. Lee, YuRalchenko, High Energy Dens. Phy. 5 (2009) 15.
[13] H.A. Scott, J. Quant, Spectrosc. Radiat. Transf. 71 (2001) 689.
[14] M.H. Chen, B. Crasemann, N. Mårtensson, B. Johansson, Phys. Rev. A 31 (1985) 556.
[15] D.A. Liberman, J.R. Albritton, B.G. Wilson, W.E. Alley, Phys. Rev. A 50 (1994) 171.
[16] O. Peyrusse, C. Bauche-Arnoult, J. Bauche, J. Phys. B 38 (2005) L137.
[17] A. Bar-Shalom, J. Oreg, M. Klapisch, J. Quant. Spectrosc. Radiat. Transf. 65 (2000) 43.
[18] F. de Gaufridy de Dortan, Rapport CEA-R 6115 (2006) 0429.
[19] J.J. MacFarlane, I.E. Golovkin, P.R. Woodfruff, et al.Proceedings of Inertial Fusion and Sciences Applications, Amer. Nucl. Soc. (2003) 457.
[20] J. Abdallah Jr., H.L. Zhang, C.J. Fontes, D.P. Kilcrease, B.J. Archer, J. Quant. Spectrosc. Radiat. Transf. 71 (2001) 107.
[21] S. Mazevet, J. Abdallah Jr., J. Phys. B: Mol. Opt. Phys. 39 (2006) 3419.
[22] F.B. Rosmej, Europhys. Lett. 76 (2006) 1081.
[23] C. Bauche-Arnoult, J. Bauche, J. Quant, Spectrosc. Radiat. Transf. 71 (2001) 189.
[24] J. Bauche, C. Bauche-Arnoult, K.B. Fournier, Phys. Rev. E 69 (2004) 026403.
[25] O. Peyrusse, C. Bauche-Arnoult, J. Bauche, Phys Plasmas 12 (2005) 063302.
[26] E.G. Hill, S.J. Rose, High Energy Dens. Phys. 5 (2009) 302.
[27] R.W. Clark, J. Davis, J.P. Apruzese, J.L. Giuliani Jr., J. Quant. Spectrosc. Radiat. Trans. 53 (1995) 307.
[28] S.B. Hansen, J. Bauche, C. Bauche-Arnoult, M.F. Gu, High Energy Dens. Phys. 3 (2007) 109.
[29] G.V. Brown, S.B. Hansen, E. Träbert, P. Beiersdorfer, K. Widmann, H. Chen, H.K. Chung, J.H.T. Clementson, M.F. Gu, D.B. Thorn, Phys. Rev. E 77 (2008) 066406.
[30] C.J. Fontes, J. Colgan, H.L. Zhang, J. Abdallah Jr., J. Quant. Spectrosc. Radiat. Transf. 99 (2006) 175.
[31] C. Bauche-Arnoult, J. Bauche, M. Klapisch, Phys. Rev. A 31 (1985) 2248.
[32] J. Bauche, C. Bauche-Arnoult, M. Klapisch, Adv. Atom Mol. Phys. 23 (1988) 131.
[33] A. Bar-Shalom, J. Oreg, W.H. Goldstein, J. Quant. Spectrosc. Radiat. Trans. 51 (1994) 27.
[34] O. Peyrusse, J. Phys., B. At, Mol, Opt. Phys. 33 (2000) 4303.
[35] F. Gilleron, J.-C. Pain, High Energy Dens. Phys. 5 (2009) 320.
[36] R.D. Cowan, The Theory of Atomic Structure and Spectra. University of California Press, Berkeley, 1981.
[37] G. Faussurier, C. Blancard, P. Renaudin, High Energy Dens. Phys. 4 (2008) 114.
[38] G. Faussurier, C. Blancard, A. Decoster, J. Quant. Spectrosc. Radiat. Transf. 58 (1997) 233.
[39] C. Bauche-Arnoult, J. Bauche, M. Klapisch, Phys. Rev. A 20 (1979) 2424.
[40] S.B. Hansen, A.Ya. Faenov, T.A. Pikuz, et al., Phys. Rev. E 72 (2005) 036408.
[41] J. Bauche, C. Bauche-Arnoult, Theory of complex spectra from laser plasmas. in: R.M. More (Ed.), Laser Interactions with Atoms, Solids and Plasmas. Plenum Press, New York, 1994.
[42] M. Poirier, F. de Gaufridy de Dortan, High Energy Dens. Phys. 5 (2009) 328.
[43] D. Liberman, J. Albritton, J. Quant. Spectrosc. Radiat. Transf. 51 (1994) 197.
[44] D.G. Hummer, D. Mihalas, Astrophys. J. 331 (1988) 794.
[45] J. Bauche, C. Bauche-Arnoult, E. Luc-Koenig, J.-F. Wyart, M. Klapisch, Phys. Rev. A 28 (1983) 829.
[46] C.J. Colgan, C.J. Fontes, J. Abdallah Jr., High Energy Dens. Phys. 2 (2006) 90.
[47] P. Mazzotta, G. Mazzitelli, S. Colafrancesco, N. Vittorio, Astron. Astro. Sup. 133 (1998) 403.
[48] P. Bryans, N.R. Badnell, T.W. Gorczyca, J.M. Laming, W. Mitthumsiri, D.W. Savin, Astrophys. J. Suppl. Ser. 167 (2006) 343.
[49] J. Bauche, C. Bauche-Arnoult, M. Klapisch, P. Mandelbaum, J.L. Schwob, J Phys B 20 (1987) 1443.
[50] J. Oreg, W.H. Goldstein, A. Bar-Shalom, M. Klapisch, Phys Rev A 39 (1989) 4599.
[51] S.B. Hansen, K.B. Fournier, C. Bauche-Arnoult, J. Bauche, O. Peyrusse, J. Quant. Spectrosc. Radiat. Transf. 99 (2006) 272.
[52] B.L. Henke, E.M. Gullikson, J.C. Davis, Atom. Data Nucl. Data Tables 54 (1993) 181.
[53] D.J. Hoarty, J.W.O. Harris, P. Graham, et al., High Energy Dens. Phys. 3 (2007) 325.

Please cite this article in press as: S.B. Hansen, et al., Superconfiguration widths and their effects on atomic models, High Energy Density Physics (2010), doi:10.1016/j.hedp.2010.07.002